Materials Horizons

COMMUNICATION

View Article Online
View Journal | View Issue

Cite this: *Mater. Horiz.*, 2015, 2, 528

Received 22nd June 2015,
Accepted 21st July 2015

DOI: 10.1039/c5mh00113g

www.rsc.li/materials-horizons

Searching beyond Gd for magnetocaloric frameworks: magnetic properties and interactions of the $Ln(HCO_2)_3$ series†

Paul J. Saines,*[a] Joseph A. M. Paddison,[ab] Peter M. M. Thygesen[a] and Matthew G. Tucker[b]

This study probes the magnetic properties and interactions of the $Ln(HCO_2)_3$ (Ln = Tb^{3+}–Er^{3+}) frameworks. We show that the magnetocaloric effect of $Tb(HCO_2)_3$ is significantly higher above 4 K in moderate magnetic fields compared to the promising $Gd(HCO_2)_3$. While the peak performance of $Tb(HCO_2)_3$ is lower than $Gd(HCO_2)_3$, we also find that the Gd-rich members of the solid solution $Gd_{1-x}Tb_x(HCO_2)_3$ blend the advantages of both end-members. Using neutron diffraction experiments, $Tb(HCO_2)_3$ is found to be antiferromagnetic below 1.7 K with ferromagnetic face-sharing chains and antiferromagnetic coupling between them. Analysis of magnetic diffuse scattering of the paramagnetic phase indicates that ferromagnetic coupling is retained, and it is likely that this plays a role in improving its magnetocaloric performance in low fields.

Conceptual insights

Alternate coolants are needed to replace the use of increasingly scarce liquid helium to reach ultra-low temperatures, required, for example, to cool superconductors used in medical resonance imaging to below 10 K. Paramagnetic magnetocalorics, which posses entropically driven cooling when in a cycled magnetic field, are one such replacement. Recently gadolinium-based coordination frameworks that have amongst the largest magnetocaloric effects have been developed; the cooling power of these materials, however, peaks below 2 K, below the temperatures required for many applications of liquid helium. This work shows that the incorporation of heavier lanthanides, in particular terbium, into a magnetocaloric framework can lead to a significant increase in their performance at higher temperatures—particularly in applied fields reachable using permanent magnets, the most practical for functional cooling devices. The detailed magnetic interactions in terbium formate have also been examined, the first study of the magnetic correlations in a paramagnetic coordination framework, which reveals that Ising-like one-dimensional ferromagnetic coupling is present in the paramagnetic phase. These interactions are likely to play a role in its excellent magnetocaloric performance by increasing its ease of magnetisation.

1. Introduction

Functional magnets have great potential to underpin the development of new technologies for a wide range of applications.[1,2] Coordination frameworks have attracted particular attention in this regard, because their unusual architectures allow them to exhibit uniquely-modified magnetic properties not found in conventional ionic solids.[2–4] Recently, frameworks have been created that exhibit the paramagnetic magnetocaloric effect (MCE),[2,5,6] an entropically-driven cooling process that occurs when paramagnets are in a cycled magnetic field. Several frameworks, including $Gd(HCO_2)_3$, have recently been reported whose MCEs are comparable or superior to $Gd_3Ga_5O_{12}$, the benchmark compound for MCE cooling below 10 K.[5,6] These materials have possible applications as ultra-low-temperature coolants, potentially replacing increasingly expensive and scarce liquid helium.[2,7] The current focus of the development of MCE frameworks lies in achieving higher maximum entropy changes – typically for temperatures below 2 K and applied magnetic fields greater than 5 T. Such materials are used as a second stage in an adiabatic demagnetisation refrigerator (ADR), with liquid helium or a cryocooler, cooling the system down to 4 K before magnetic cooling enables the sample environment to be cooled below 1 K, typically for scientific observation. Given the increasing scarcity of liquid helium and complexity and reliability issues of multistage cryocoolers, which are necessary to reach 4 K, the development of magnetocaloric compounds that operate more efficiently at moderately higher temperatures may be useful when combined with a single stage cryocooler capable of reaching 10–20 K.[8] Ideally, this would be accompanied by having as large an MCE as possible in lower applied fields, particularly below the typical 2 T field limits of permanent magnets.[5,9] This could allow more economical devices to be created for many applications requiring cooling in the 4–10 K range, *e.g.* cooling the niobium superconducting magnets used in medical resonance imaging and nuclear magnetic resonance facilities.[10]

Very little is known regarding how the paramagnetic interactions in magnetocalorics relate to their fascinating properties.

[a] *Department of Chemistry, University of Oxford, Inorganic Chemistry Laboratory, South Parks Road, Oxford, OX1 3QR, UK. E-mail: paul.saines@chem.ox.ac.uk*
[b] *ISIS Facility, Rutherford Appleton Laboratory, Harwell Oxford, Didcot, OX1 3QR, UK*
† Electronic supplementary information (ESI) available. See DOI: 10.1039/c5mh00113g

Neutron scattering is the method of choice for probing magnetic interactions and has recently begun to be applied to study magnetically-ordered frameworks;[4,11] its application, however, to magnetocalorics and other low dimensional and frustrated frameworks is very limited.[12] This is because sufficiently large single crystals of coordination frameworks are seldom available, and it has long been considered that little information about the paramagnetic state can be extracted using neutron powder diffraction. While the very large neutron-absorption cross section of Gd also typically restricts studying many magnetocalorics, recent studies have shown that this problem is surmountable.[13] Our research on frustrated and disordered magnets has shown that significantly more information can be obtained from powder magnetic diffuse scattering than has traditionally been anticipated.[14,15] Applying such techniques to frameworks would enable a much deeper understanding of their low dimensional or frustrated behaviour.

Here we present a survey of the magnetic properties of the $Ln(HCO_2)_3$ (Ln = Tb^{3+}, Dy^{3+}, Ho^{3+} and Er^{3+}) frameworks. Unexpectedly, we reveal that $Tb(HCO_2)_3$ has a larger MCE than $Gd(HCO_2)_3$ for temperatures between 4 and 10 K and applied fields below 2 T. Doping across the $Gd_{1-x}Tb_x(HCO_2)_3$ solid solution series is found to further optimize the MCE properties of this family. Encouraged by the properties of $Tb(HCO_2)_3$, we also investigated its magnetic interactions using neutron diffraction, characterising both its long-range magnetic order present below 1.7 K and the short-range order in its paramagnetic phase—the first time that such a study has been completed on a coordination framework. We show that ferromagnetic coupling within the TbO_9 chains in $Tb(HCO_2)_3$ is the dominant interaction in the paramagnetic phase, which may play a role in its interesting magnetocaloric properties.

2. Experimental

Samples were synthesised by slowly adding 1 g of the appropriate $Ln(NO_3)_3{\cdot}xH_2O$ (99.9%, x = 6 for Ln = Gd^{3+} or Tb^{3+}, Sigma-Aldrich, and x = 5 for Ln = Dy^{3+}, Ho^{3+} and Er^{3+}, Alfa Aesar) to 5 mL of formic acid (Sigma-Aldrich, 95% reagent grade) in a 30 mL tall glass vial. This was stirred overnight and the product filtered off, washing with ethanol. $Gd_{1-x}Tb_x(HCO_2)_3$ was made by reactions carried out with finely ground stoichiometric mixtures of $Gd(NO_3)_3$ and $Tb(NO_3)_3$. The 5 g sample of $Tb(DCO_2)_3$ used for neutron diffraction was made using the same method but was a combination of three batches made using 4 g of $Tb(NO_3)_3{\cdot}6H_2O$ and perdeuterated formic acid (Sigma-Aldrich 95% in D_2O, 98% D). Sample purity was examined by powder X-ray diffraction, using a Bragg–Brentano PANalytical Empyrean diffractometer equipped with Cu-Kα_1 radiation and a PIXcel detector. Dc magnetisation data were collected using a Quantum Design MPMS 5 XL SQUID magnetometer with powder samples contained in gel caps and held in a straw with a uniform diamagnetic background.

Time-of-flight neutron powder diffraction patterns were recorded using the GEM diffractometer at the ISIS neutron facility, Rutherford Appleton Laboratories, UK.[16] Data covered a reciprocal-space range $0.25 < Q < 25$ Å^{-1} and were measured at temperatures between 1.4 K and 300 K for 30 μAh (900 μAh at 3 K). The sample was cooled in an 8 mm V can in an Oxford Instruments Variox Cryostat. Data were fitted using the GSAS Rietveld refinement package using the EXPGUI interface.[17] Refinements were carried out with a profile function featuring a convolution of back-to-back exponentials with a pseudo-Voigt model, with backgrounds fitted using shifted Chebyschev polynomials. Refinement of the D fractional occupancy showed that the sample is perdeuterated.

Likely magnetic structures for the ordered phase were determined using the ISODISTORT software suite[18] by exploring the magnetic distortion modes and symmetries consistent with the observed magnetic propagation vector, **k**, and the parent crystal structure. In order to characterise short-range spin correlations in the paramagnetic state, magnetic diffuse scattering data were obtained from the lowest-Q detector bank (bank 1) on GEM. Bragg scattering, as determined from Rietveld refinements, and experimentally measured background contributions, including from the sample environment, were subtracted. The resulting magnetic diffuse-scattering data were fitted using the Spinvert Reverse Monte Carlo (RMC) refinement package.[15] In RMC refinement, spin orientations in a periodic supercell are fitted to diffuse-scattering data using a Metropolis Monte Carlo algorithm. We used a 5 × 3 × 13 size metrically-orthorhombic supercell related to the trigonal cell by a basis vector of [(1, 0, 0),(1/3, 2/3, 0),(0, 0, 1)]. The magnetic form factor of Tb^{3+} was obtained from tabulated coefficients.[19] The phase scale and a flat background term were also refined.

3. Results and discussion

3.1 Magnetic properties of the $Ln(HCO_2)_3$ frameworks

Rietveld fits to X-ray diffraction data confirmed that all samples used in this study were phase pure and adopt the known rhombohedral *R3m* structure under ambient conditions (see Fig. S1–S5, ESI†).[5] In this structure the LnO_9 polyhedra are connected into face-sharing chains down the *c*-axis with these chains interconnected *via* the formate ligand into a triangular arrangement (see Fig. 1). There are two different oxygen cations in the structure, bonding to one and two Ln^{3+} cations, respectively, with the latter anion connecting the Ln^{3+} cations in a chain. The triangle connections of the Ln^{3+} cation are not equilateral but instead feature two short bonds and one long bond, which rotate between adjacent layers along the *c*-axis.

Field cooled (FC) and zero-field cooled (ZFC) magnetic susceptibility data of the $Ln(HCO_2)_3$ frameworks (Ln = Gd^{3+}, Tb^{3+}, Dy^{3+}, Ho^{3+} and Er^{3+}) were measured in a 100 Oe field from 2 K to 300 K and did not show any indication of long range magnetic order. These data were well fitted using the Curie–Weiss law (see Fig. S6–S10, ESI†) with Curie–Weiss temperatures of −0.6 K, −0.9 K, −6.1 K, −10.3 K and −16.0 K, for Gd^{3+}–Er^{3+}. $Gd(HCO_2)_3$, therefore, has antiferromagnetic interactions but the significant orbital moment of the other lanthanides

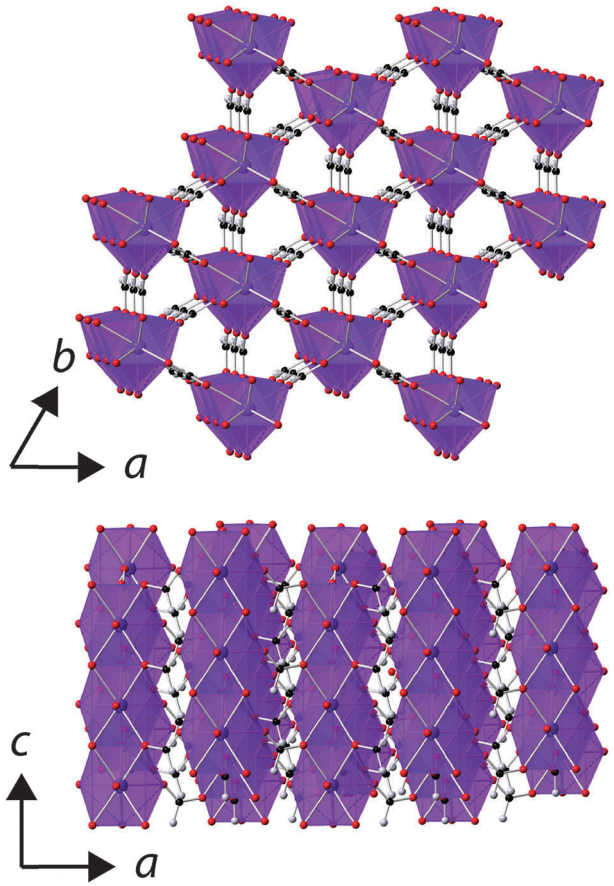

Fig. 1 The structure of the $Ln(HCO_2)_3$ frameworks. The Ln^{3+}, oxygen, carbon and hydrogen atoms are represented in purple, red, black and grey, respectively.

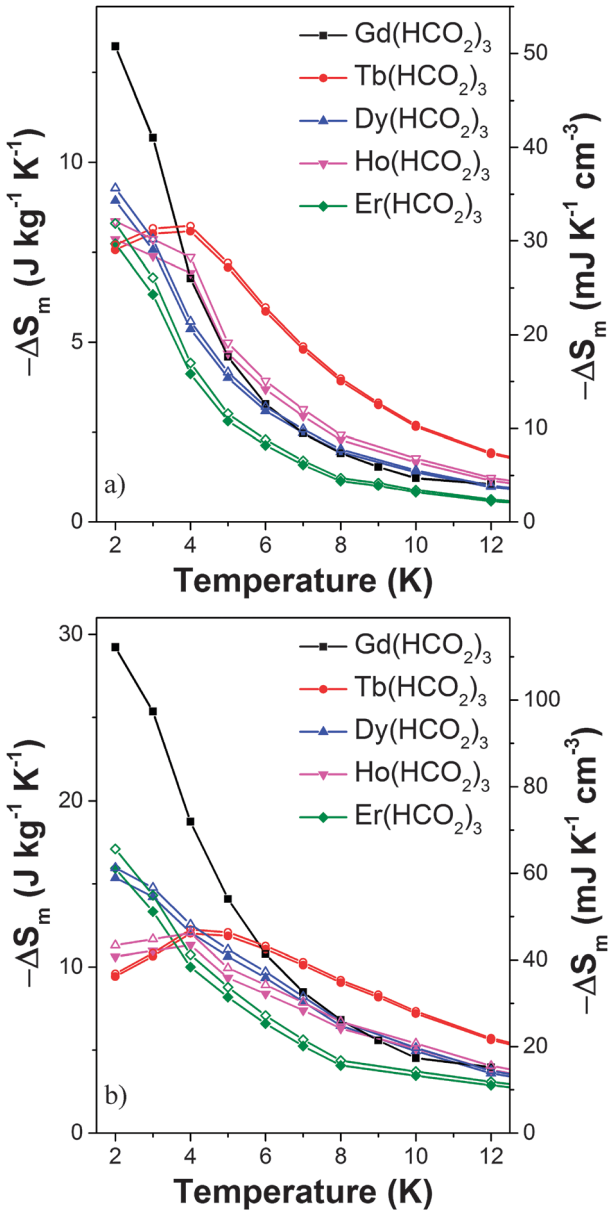

Fig. 2 Magnetic entropy change for the $Ln(HCO_2)_3$ frameworks for (a) ΔB = 1–0 T and (b) ΔB = 2–0 T. The filled and hollow symbols mark mass and volumetric units, respectively.

means their Curie–Weiss temperatures are a sum of any magnetic interactions and the effect of depopulation of the Stark levels so a similar analysis cannot be made. Effective magnetic moments were found to be broadly consistent with the values expected for these trivalent lanthanides according to the Russell–Saunders coupling scheme, with values of 7.86, 9.62, 10.00, 10.48 and 9.68 μ_B obtained. Magnetisation measurements exhibit paramagnetic behaviour and appear close to saturation under an applied field of 5 T (see Fig. S11–S16, ESI†). Interestingly, $Tb(HCO_2)_3$ appears close to saturation at 1 T, a much lower field than its Gd^{3+} analogue despite its higher magnetic anisotropy (discussed below); this greater ease of magnetisation increases further with increasing temperature.

Magnetic entropy change, ΔS_m, was calculated from the Maxwell relation $\Delta S_m(T) = \int[\partial M(T,B)/\partial T]_B dB$ from 2 K to 12 K for ΔB = 5–0 T. This gave $-\Delta S_m^{max}$ of 15.7, 20.8, 14.7 and 19.2 J kg^{-1} K^{-1} for Tb^{3+}, Dy^{3+}, Ho^{3+} and Er^{3+}, with T_{max} of 7, 6, 4 and 2 K, corresponding to volumetric values of $-\Delta S_m^{max}$ of 61.3, 82.9, 60.1 and 79.1 mJ cm^{-3} K^{-1} (see Fig. S17, ESI†). These $-\Delta S_m$ values are all significantly lower than the 190.4 mJ cm^{-3} K^{-1} we obtain for $Gd(HCO_2)_3$ with T_{max} = 2 K for ΔB = 5–0 T, which is close to the value found in a previous study.[5] The higher T_{max} temperatures of the other lanthanides, particularly Tb^{3+}, attracted our attention. Indeed, for ΔB = 1–0 T the $-\Delta S_m$ of $Tb(HCO_2)_3$ is significantly higher than that of $Gd(HCO_2)_3$ above 4 K. The same is true for $Ho(HCO_2)_3$, albeit to a very small extent (see Fig. 2a). A greater $-\Delta S_m$ is also observed for $Tb(HCO_2)_3$ for ΔB = 2–0 T above 6 K, although the differences in the values achieved compared to the Gd^{3+} compound are smaller (see Fig. 2b). This result highlights that the incorporation of Tb^{3+} cations into coordination frameworks allows their MCE properties to be optimised at higher temperatures and in lower applied fields, compared to the corresponding Gd^{3+} compound. Previous studies of $Gd_{1-x}Tb_xGa_5O_{12}$ showed the same effect, but by a much smaller margin.[20] This is significant as many of the applications of liquid helium do not require

cooling below 4 K, which most paramagnetic MCE materials are optimised for. It should be noted here that the magnetocaloric effect can be probed directly from heat capacity measurements, which is desirable particularly when determining the specific heat transfer, ΔQ.[21] Recent work on $Gd(HCO_2)_3$ and $GdOH(CO_3)$, however, have shown that for similar frameworks excellent agreement is usually obtained between the direct determination of $-\Delta S_m$ and the indirect method presented in this work.

Since the incorporation of Tb^{3+} yielded improved MCE properties at higher temperatures compared to $Gd(HCO_2)_3$ but lower $-\Delta S_m^{max}$, the magnetic properties of the $Gd_{1-x}Tb_x(HCO_2)_3$ (x = 0.2, 0.4, 0.6 and 0.8) solid solution were investigated. High-resolution X-ray diffraction indicate these compounds are pure single phases, although there was some evidence of peak broadening, suggesting that they exhibit a degree of strain or cation inhomogeneity (see Fig. S18, ESI†). Magnetic susceptibilities were well fitted by Curie–Weiss law, yielding effective magnetic moments consistent with stoichiometries of x = 0.19, 0.40, 0.57 and 0.76 across the series, close to the expected nominal stoichiometries. The Curie–Weiss temperatures were −0.9 K for the whole series except for $Gd_{0.4}Tb_{0.6}(HCO_2)_3$, which had a value of −1.3 K. Only $Gd_{0.4}Tb_{0.6}(HCO_2)_3$ varied from mean-field behaviour, with an antiferromagnetic cusp present in ZFC measurements at 3 K that is not observed in FC data (see Fig. S19, ESI†); magnetization measurements at 2 K are consistent with paramagnetic behaviour suggesting $Gd_{0.4}Tb_{0.6}(HCO_2)_3$ is not a simple antiferromagnet.

For the x = 0.2 and 0.4 members of the $Gd_{1-x}Tb_x(HCO_2)_3$ series the $-\Delta S_m$ for ΔB = 1–0 T are significantly higher than would be expected for a physical mix of the two end-member phases. This is particularly significant for $Gd_{0.8}Tb_{0.2}(HCO_2)_3$ as at 2 K, the lowest temperature probed its $-\Delta S_m$ for a ΔB = 1–0 T is equal to that of $Gd(HCO_2)_3$. It decreases more slowly than for the pure Gd phase, such that for temperatures above 5 K its $-\Delta S_m$ is between 10–15% higher (see Fig. 3 and Fig. S20–S23 for magnetisation data, ESI†). Similarly, while the $-\Delta S_m^{max}$ for $Gd_{0.6}Tb_{0.4}(HCO_2)_3$ is about 10% lower than $Gd(HCO_2)_3$ for a ΔB = 1–0 T above 5 K, its $-\Delta S_m$ is between 14 to 24% higher. The performance of both doped compounds also exceeds that of $Gd(HCO_2)_3$ at higher temperatures for a ΔB = 2–0 T, although this is only above 6 and 7 K for x = 0.2 and x = 0.4, respectively, and the difference remains less than 10%. To the best of our knowledge this is the first study of the magnetocaloric properties of a framework solid solution and has shown the potential advantages of such an approach to optimise the physical properties of such materials – namely, retaining most of the performance of $Gd(HCO_2)_3$ in low fields, while improving on its MCE at moderately higher temperatures.

3.2 Magneto-structural characterisation of $Tb(DCO_2)_3$

The interesting properties of $Tb(HCO_2)_3$ encouraged further investigation of its structure and magnetic interactions using neutron diffraction, particularly in the paramagnetic phase. Past studies of the $Ln(HCO_2)_3$ frameworks have suggested a subtle structural transition occurs below 150 K due to a very small reduction ($\approx$0.05%) of the c-axis in $Tm(DCO_2)_3$[22] and features observed in Raman spectra of $Pr(HCO_2)_3$.[23] The proposed

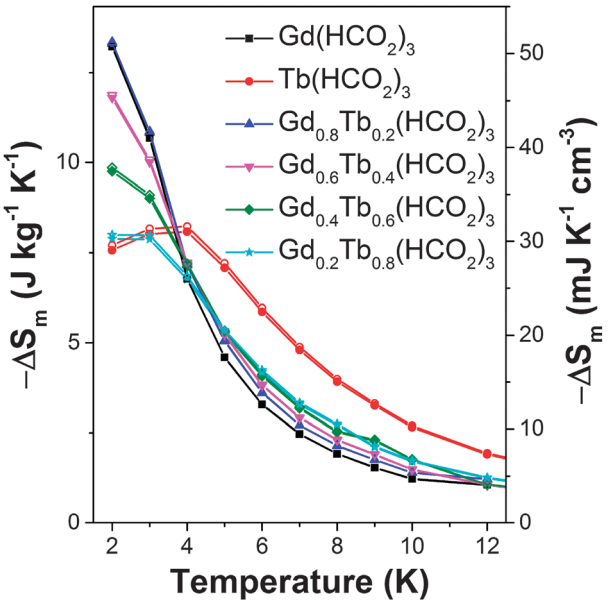

Fig. 3 Magnetic entropy change for the $Gd_{1-x}Tb_x(HCO_2)_3$ series for ΔB = 1–0 T. The filled and hollow symbols mark mass and volumetric units, respectively.

transition is from the ambient temperature $R3m$ rhombohedral structure to $R3$ symmetry and involves a rotation of the formate groups.[23] Neutron diffraction should be particularly sensitive to such a transition, as it will involve a significant movement of the deuterium atoms. We find a similar minute change in the lattice parameters of $Tb(DCO_2)_3$ below 80 K (see Fig. S24, ESI†), but Rietveld refinements to the data collected at 3 K using both possible space groups give equivalent excellent fits: for $R3$, R_p = 1.60% and R_{wp} = 2.26%, and for $R3m$, R_p = 1.67% and R_{wp} = 2.30%. Moreover, the maximum displacement of each atom in the $R3$ structure is within 0.1 Å of the position required by $R3m$ symmetry. We therefore conclude that $R3m$ symmetry is retained to 3 K (see Tables S1–S4 for crystallographic details and selected bond distances and angles determined at 3 and 300 K, ESI†). There are no significant changes observed that indicate the cause of the subtle change in the c-axis length. There is also no indication of diffuse scattering appearing above 10 K, so it is unlikely to be related to structural disorder.

A neutron diffraction pattern obtained from $Tb(DCO_2)_3$ at 1.4 K revealed the presence of additional reflections, especially at high d-spacing (see Fig. 4), consistent with the emergence of magnetic order. These were found to index on the parent cell but violated the rhombohedral centering conditions. This is consistent with the magnetic structure of $Tb(DCO_2)_3$ belonging to the **k**-vector Λ, (0, 0, g), which is allowed to be incommensurate but here appears to have locked into a commensurate value of g = 1. Of the possible magnetic structures suggested by ISODISTORT only those belonging to the magnetic space group $P3m'1$ fitted the data. There were two possible magnetic structures of this type, each of which have ferromagnetic face-sharing chains, with spins found to align along the c-axis. One possible structure has three ferromagnetic chains with

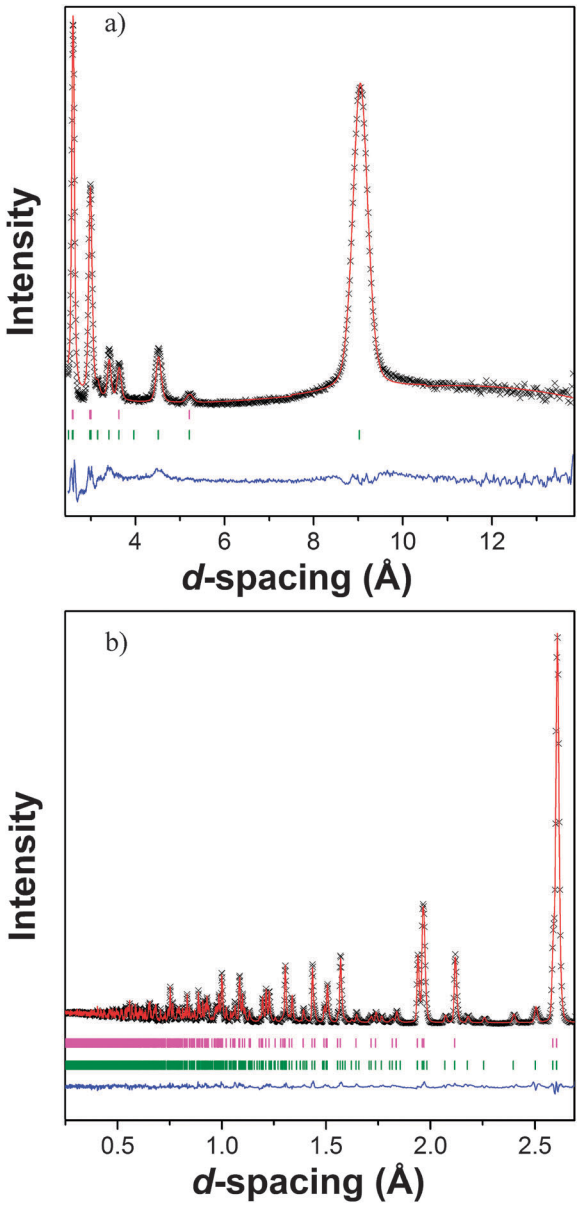

Fig. 4 Neutron diffraction pattern collected from $Tb(DCO_2)_3$ at 1.4 K using (a) bank 2 and (b) bank 5 of the GEM diffractometer fitted using the Rietveld method. The crosses, upper and lower lines indicate the observed and calculated intensities and the differences between these. The upper and lower sets of vertical markers indicate those allowed by the nuclear and magnetic structures.

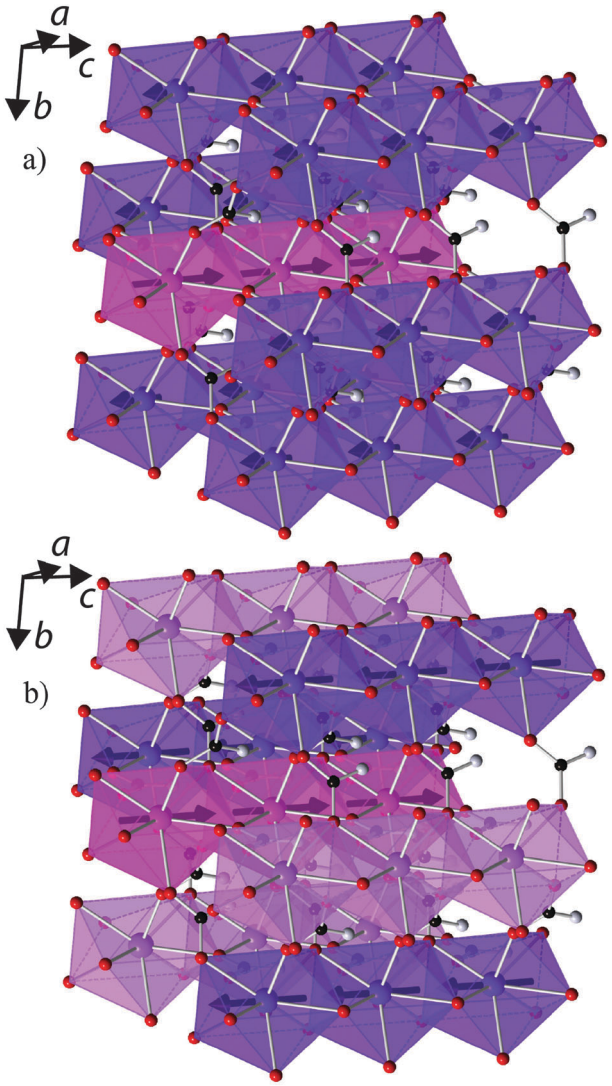

Fig. 5 The two possible magnetic structures of $Tb(DCO_2)_3$. The distinct Tb^{3+} cations are shown in different colours with the ordered spin direction indicated by the arrows pointing through them. All other colours are the same as in Fig. 1.

one chain having twice the magnetic moment of the others and coupled antiferromagnetically to them (see Fig. 5a). This model is consistent with that proposed in a previous study of Kurbakov *et al.*,[24] who briefly analysed the magnetic structure of $Tb(DCO_2)_3$ using a basis vector approach. The other structure has the spins in two ferromagnetic chains coupled antiferromagnetically to each other with the remaining chain being disordered (see Fig. 5b), a so-called spin-idle structure. The fits of these two structures to the 1.4 K data are equivalent (R_p = 1.94% for both models and R_{wp} = 2.09% and 2.10% for the spin-idle and unequal spin structure, respectively). The largest magnetic moment is 5.91 μ_B and 6.80 μ_B for the spin-idle and unequal-spin structure, respectively. These values are well below the expected magnetic moment of 9.72 μ_B for isotropic Tb^{3+} moments, consistent with the observation of magnetic diffuse scattering, which persists more weakly up to 10 K. Magnetic reflections appear between 1.65 and 1.72 K, indicating the onset of magnetic order (see Fig. S25 for the evolution of the magnetic moments, ESI†). The square of the observed magnetic moment is proportional to the Landau order parameter, Q; a good linear fit to the square of the ordered magnetic moment is obtained, confirming that the magnetic-ordering transition is second order and occurs at 1.72(12) K.

Both possible magnetic structures of $Tb(DCO_2)_3$ indicate that the dominant intra-chain coupling is ferromagnetic, consistent with the small Tb–O2–Tb bond angle of 105.79(4)°. As the intra-chain super-exchange distances are much smaller than those

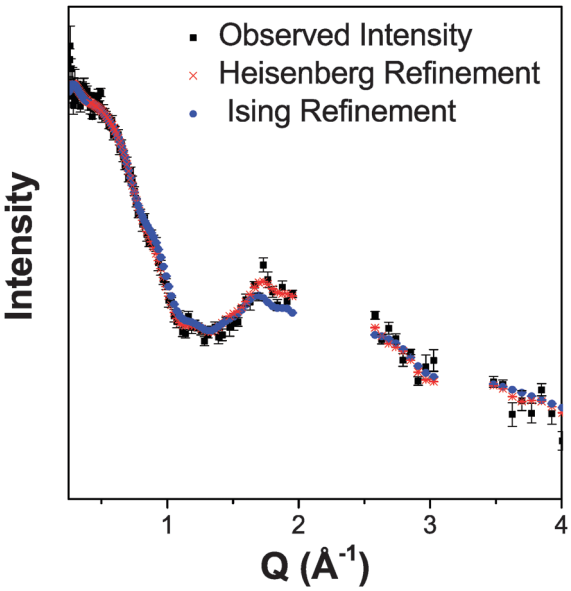

Fig. 6 Comparison of the Heisenberg-like and Ising-like RMC fits to the neutron diffuse scattering of $Tb(DCO_2)_3$ at 3 K. The results are averaged over ten refinements.

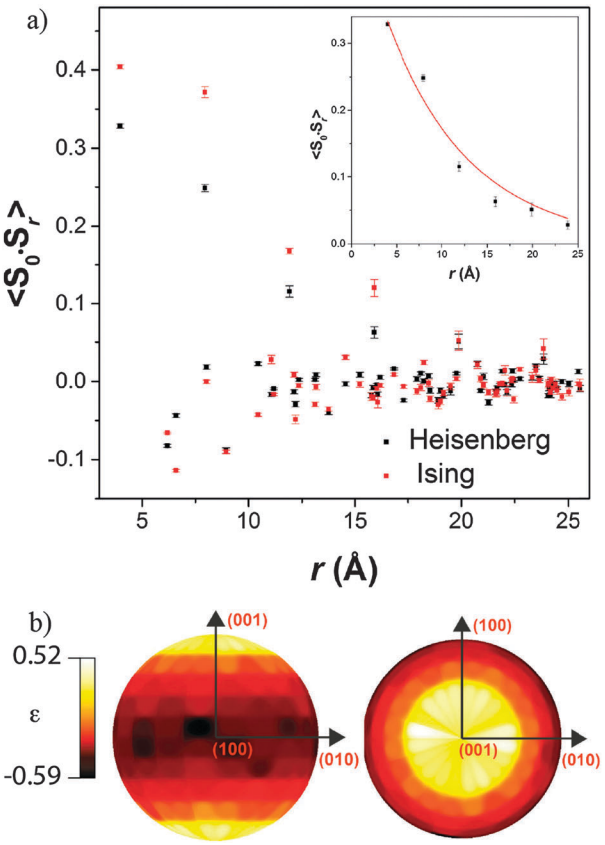

Fig. 7 Depictions of (a) $\langle S_0 \cdot S_r \rangle$ correlations averaged over ten RMC refinements with an inset showing a exponential correlation length fit to the ferromagnetic intra-chain interactions and (b) stereographic projections of the spin orientations averaged over 100 RMC Heisenberg-like fits to diffuse neutron scattering data from $Tb(DCO_2)_3$ at 3 K. The relative spin density, $\varepsilon(\theta, \phi)$, is defined as $\varepsilon(\theta, \phi) = \ln\left[\frac{n(\theta, \phi)}{N \mathrm{d}(\cos\theta)\mathrm{d}\phi}\right]$, where $n(\theta, \phi)$ is the number of spins with orientations within the range $\mathrm{d}(\cos\theta)$, $\mathrm{d}\phi$.

between chains (*cf.* 4.98 Å to 7.42 Å), it would be expected that this compound will resemble a one-dimensional system above its long-range ordering temperature. Fits to the diffuse magnetic scattering observed at 3 K using RMC refinement confirm that this is the case (see Fig. 6 for the quality of fit). Initially, unconstrained refinements were performed in which the spins were allowed to point in any direction, in a Heisenberg-like fashion. A plot of $\langle S_0 \cdot S_r \rangle$ averaged over ten such refinements show that the dominant spin correlations in this material are ferromagnetic within the chains (see Fig. 7a), with a correlation length of 9.2(1.3) Å. The inter-chain correlations are much weaker and antiferromagnetic, with $\langle S_0 \cdot S_r \rangle$ correlations of $-0.082(2)$ and $-0.044(3)$ observed for Tb^{3+} cations separated by the shorter, 6.16 Å and longer, 6.57 Å distances found in the triangles, respectively.

Stereographic projections of the refined spin orientations indicate that even well above the magnetic ordering temperatures the spins are preferentially aligned along the *c*-axis (see Fig. 7b), indicating an Ising-like magnetic anisotropy. Attempts were therefore made to fit the diffuse scattering data with Ising spins constrained to point along the *c*-axis. The Ising refinements also yielded a reasonable fit, though of somewhat lower quality than the unconstrained refinement (*cf.* χ^2 of 290 and 414 for ten averaged Heisenberg and Ising fits, respectively), which would be expected as the Ising refinement is more highly constrained. This result suggests that the spins have a strong, although probably not purely, Ising character. To the best of our knowledge this is the first RMC study of the magnetic interactions in the paramagnetic phase of a coordination framework.

The significant ferromagnetic intra-chain interactions in the paramagnetic phase of $Tb(HCO_2)_3$ explain the relative ease of its magnetization compared to $Gd(HCO_2)_3$, whose negative Curie–Weiss temperature indicates predominantly antiferromagnetic interactions. It can be envisaged that the strong ferromagnetic intra-chain interactions, present on a local scale of about 10 Å, will lead to the Tb^{3+} spins aligning readily with an applied magnetic field, easily overcoming the much weaker inter-chain antiferromagnetic coupling. Bulk measurements show that this greater ease of magnetization is retained to higher temperature, leading to a higher peak temperature for $-\Delta S_m^{max}$ than found in $Gd(HCO_2)_3$, which may make $Tb(HCO_2)_3$ suitable for cooling applications at moderately higher temperatures. The trade-off for this is a lower $-\Delta S_m^{max}$ compared to $Gd(HCO_2)_3$, due to a combination of its lower magnetic moment and a more gradual change of magnetisation with temperature. In the $Gd_{1-x}Tb_x(HCO_2)_3$ solid solution a mixture of these two cations leads to a retention of most of the peak performance of the $Gd(HCO_2)_3$ but a slower reduction in $-\Delta S_m$ with temperature in low applied fields. While to date the development of magnetocaloric frameworks has focused on Gd^{3+} containing-compounds, this study highlights the benefits of incorporating heavier lanthanides into framework structures known to have excellent magnetocaloric properties. By combining a deeper understanding of their magnetic interactions with judicious choices of doping in

solid solutions, it should be possible to expand the palate of available magnetocaloric frameworks and optimize their application.

4. Conclusion

In this work we have reported the MCE of the $Ln(HCO_2)_3$ (Ln = Tb^{3+}, Dy^{3+}, Ho^{3+} and Er^{3+}) frameworks for the first time and compared them to the properties of the related $Gd(HCO_2)_3$, which is already proven to be an excellent candidate as a magnetocaloric material.[5] We have shown that, although the peak performance of the other lanthanide formates is not as great as for $Gd(HCO_2)_3$, the temperature at which their performance peaks is significantly higher. This is particularly important in the case of the Tb^{3+} compound, which significantly outperforms $Gd(HCO_2)_3$ above 4 K in fields below 2 T, the maximum field typically achievable with permanent magnets. Moreover, we show that the Gd^{3+}-rich end-members of the solid solution $Gd_{1-x}Tb_x(HCO_2)_3$ retain much or all of the peak performance of $Gd(HCO_2)_3$ but also exhibit a slower decline in their $-\Delta S_m$, leading to better performance. The magnetic order of $Tb(DCO_2)_3$ in both its antiferromagnetic and paramagnetic phases has also been examined. We find that the Tb^{3+} spins in the edge-sharing chains order ferromagnetically below 1.7 K into an arrangement featuring antiferromagnetic triangles. Only partial order occurs, indicating the inherent frustration in this system, and significant magnetic diffuse scattering therefore remains. Fitting magnetic diffuse scattering in the paramagnetic phase, suggests that the compound resembles a one-dimensional ferromagnetic chain with magnetic moments oriented along the *c*-axis as in the ordered phase, which increases its ease of magnetisation and thereby magnetocaloric properties.

Acknowledgements

Experiments at the ISIS Pulsed Neutron Source were supported by a beamtime allocation from the Science and Technology Facilities Council. PJS would like to thank the Glasstone Bequest for financial support through the provision of a Glasstone Fellowship and Professor Andrew Goodwin for helpful discussions.

References

1 (*a*) J. Glanz, *Science*, 1998, **279**, 2045; (*b*) G. J. Halder, C. J. Kepert, B. Moubaraki, K. S. Murray and J. D. Cashion, *Science*, 2002, **298**, 1762–1765; (*c*) D. Maspoch, D. Ruiz-Molina, K. Wurst, N. Domingo, M. Cavallini, F. Biscarini, J. Tejada, C. Rovira and J. Veciana, *Nat. Mater.*, 2003, **2**, 190–195; (*d*) W. Eerenstein, N. D. Mathur and J. F. Scott, *Nature*, 2006, **442**, 759–765.

2 Y.-Z. Zheng, G.-J. Zhou, Z. Zheng and R. E. P. Winpenny, *Chem. Soc. Rev.*, 2014, **43**, 1462–1475.

3 (*a*) M. Kurmoo, H. Kumagai, K. W. Chapman and C. J. Kepert, *Chem. Commun.*, 2005, 3012–3014; (*b*) M. Kurmoo, *Chem. Soc. Rev.*, 2009, **38**, 1353–1379; (*c*) G. Rogez, N. Viart and M. Drillon, *Angew. Chem., Int. Ed.*, 2010, **49**, 1921–1923; (*d*) Z. Wang, K. Hu, S. Gao and H. Kobayashi, *Adv. Mater.*, 2010, **22**, 1526–1533; (*e*) P. J. Saines, M. Steinmann, J.-C. Tan, W. Li, P. T. Barton and A. K. Cheetham, *Inorg. Chem.*, 2012, **51**, 11198–11209; (*f*) P. J. Saines, P. T. Barton, P. Jain and A. K. Cheetham, *CrystEngComm*, 2012, **14**, 2711–2720.

4 P. J. Saines, P. T. Barton, M. Jura, K. S. Knight and A. K. Cheetham, *Mater. Horiz.*, 2014, **1**, 332–337.

5 G. Lorusso, J. W. Sharples, E. Palacios, O. Roubeau, E. K. Brechin, R. Sessoli, A. Rossin, F. Tuna, E. J. L. McInnes, D. Collison and M. Evangelisti, *Adv. Mater.*, 2013, **25**, 4653–4656.

6 (*a*) S. Biswas, H. S. Jena, A. Adhikary and S. Konar, *Inorg. Chem.*, 2014, **53**, 3926–3928; (*b*) Y.-C. Chen, L. Qin, Z.-S. Meng, D.-F. Yang, C. Wu, Z. Fu, Y.-Z. Zheng, J.-L. Liu, R. Tarasenko, M. Orendac, J. Prokleska, V. Sechovsky and M.-L. Tong, *J. Mater. Chem. A*, 2014, **2**, 9851–9858; (*c*) Y. Meng, Y.-C. Chen, Z.-M. Zhang, Z.-J. Lin and M.-L. Tong, *Inorg. Chem.*, 2014, **53**, 9052–9057.

7 M. Evangelisti and E. K. Brechin, *Dalton Trans.*, 2010, **39**, 4672–4676.

8 (*a*) Z. H. Gan, W. Q. Dong, L. M. Qiu, X. B. Zhang, H. Sun, Y. L. He and R. Radebaugh, *Cryogenics*, 2009, **49**, 198–201; (*b*) L. Chen, H. Jin, J. Wang, Y. Zhou, W. Zhu and Q. Zhou, *Cryogenics*, 2013, **54**, 54–58; (*c*) K. Yamada, *Cryogenics*, 2014, **63**, 110–113.

9 (*a*) K. A. GschneidnerJr, V. K. Pecharsky and A. O. Tsokol, *Rep. Prog. Phys.*, 2005, **68**, 1479; (*b*) A. Smith, C. R. H. Bahl, R. Bjørk, K. Engelbrecht, K. K. Nielsen and N. Pryds, *Adv. Energy Mater.*, 2012, **2**, 1288–1318.

10 L. Yuri, S. Ernst Wolfgang and Z. Tao, *Supercond. Sci. Technol.*, 2013, **26**, 093001.

11 (*a*) P. J. Saines, J. R. Hester and A. K. Cheetham, *Phys. Rev. B: Condens. Matter Mater. Phys.*, 2010, **82**, 144435; (*b*) O. Fabelo, L. Cañadillas-Delgado, I. Puente Orench, J. A. Rodríguez-Velamazán, J. Campo and J. Rodríguez-Carvajal, *Inorg. Chem.*, 2011, **50**, 7129–7135; (*c*) P. J. Saines, H. H. M. Yeung, J. R. Hester, A. R. Lennie and A. K. Cheetham, *Dalton Trans.*, 2011, **40**, 6401–6410; (*d*) L. Cañadillas-Delgado, O. Fabelo, J. A. Rodríguez-Velamazán, M.-H. Lemée-Cailleau, S. A. Mason, E. Pardo, F. Lloret, J.-P. Zhao, X.-H. Bu, V. Simonet, C. V. Colin and J. Rodríguez-Carvajal, *J. Am. Chem. Soc.*, 2012, **134**, 19772–19781; (*e*) R. A. Mole, M. A. Nadeem, J. A. Stride, V. K. Peterson and P. T. Wood, *Inorg. Chem.*, 2013, **52**, 13462–13468; (*f*) J. M. M. Lawler, P. Manuel, A. L. Thompson and P. J. Saines, *Dalton Trans.*, 2015, **44**, 11613–11620.

12 A. Kumar, S. M. Yusuf, L. Keller, J. V. Yakhmi, J. K. Srivastava and P. L. Paulose, *Phys. Rev. B: Condens. Matter Mater. Phys.*, 2007, **75**, 224419.

13 (*a*) O. A. Petrenko, C. Ritter, M. Yethiraj and D. McK Paul, *Phys. Rev. Lett.*, 1998, **80**, 4570–4573; (*b*) E. Reynolds, P. E. R. Blanchard, B. J. Kennedy, C. D. Ling, S. Liu, M. Avdeev, Z. Zhang, G. J. Cuello, A. Tadich and L.-Y. Jang, *Inorg. Chem.*, 2013, **52**, 8409–8415; (*c*) E. Palacios, J. A. Rodríguez-Velamazán, M. Evangelisti, G. J. McIntyre, G. Lorusso, D. Visser, L. J. de Jongh and L. A. Boatner, *Phys. Rev. B: Condens. Matter Mater. Phys.*, 2014, **90**, 214423.

14 (*a*) A. M. Hallas, J. A. M. Paddison, H. J. Silverstein, A. L. Goodwin, J. R. Stewart, A. R. Wildes, J. G. Cheng,

J. S. Zhou, J. B. Goodenough, E. S. Choi, G. Ehlers, J. S. Gardner, C. R. Wiebe and H. D. Zhou, *Phys. Rev. B: Condens. Matter Mater. Phys.*, 2012, **86**, 134431; (*b*) J. A. M. Paddison and A. L. Goodwin, *Phys. Rev. Lett.*, 2012, **108**, 017204; (*c*) P. J. Saines, M. G. Tucker, D. A. Keen, A. K. Cheetham and A. L. Goodwin, *Phys. Rev. B: Condens. Matter Mater. Phys.*, 2013, **88**, 134418; (*d*) J. A. M. Paddison, S. Agrestini, M. R. Lees, C. L. Fleck, P. P. Deen, A. L. Goodwin, J. R. Stewart and O. A. Petrenko, *Phys. Rev. B: Condens. Matter Mater. Phys.*, 2014, **90**, 014411.

15 J. A. M. Paddison, J. R. Stewart and A. L. Goodwin, *J. Phys.: Condens. Matter*, 2013, **25**, 454220.

16 A. C. Hannon, *Nucl. Instrum. Methods Phys. Res., Sect. A*, 2005, **551**, 88–107.

17 B. Toby, *J. Appl. Crystallogr.*, 2001, **34**, 210–213.

18 B. J. Campbell, H. T. Stokes, D. E. Tanner and D. M. Hatch, *J. Appl. Crystallogr.*, 2006, **39**, 607–614.

19 P. J. Brown, Magnetic Form Factors, http://www.ill.eu/sites/ccsl/ffacts/ffachtml.html, 2015.

20 C. P. Reshmi, S. Savitha Pillai, K. G. Suresh and M. R. Varma, *J. Magn. Magn. Mater.*, 2012, **324**, 1962–1966.

21 V. Khovaylo, *J. Alloys Compd.*, 2013, **577**, S362–S366.

22 V. Trounov, E. Tserkovnaya, S. Gavrilov and S. Vahrushev, *Physica B*, 1997, **234–236**, 679–681.

23 M. R. Moura, A. P. Ayala, J. Mendes Filho, I. Guedes, C. W. A. Paschoal, A. G. Leyva, G. Polla, D. Vega, P. K. de Perazzo and H. Lanza, *J. Raman Spectrosc.*, 2004, **35**, 159–164.

24 A. I. Kurbakov, J. Rodriguez-Carvajal, V. Trounov and N. V. Starostina, *Mater. Sci. Forum*, 2000, **321–324**, 971–975.